Fundamental Understanding of CH_4-CO_2-H_2O Interactions in Shale Nanopores under Reservoir Conditions

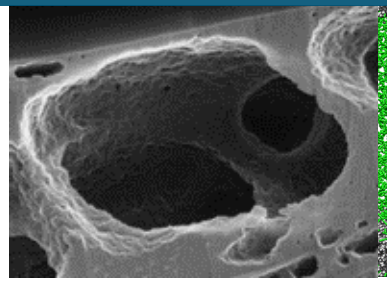

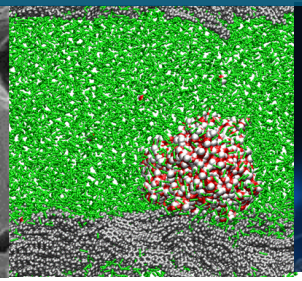

PRESENTED BY

Yifeng Wang, Tuan Anh Ho, Guangping Xu, Philippe Weck (SNL)

Shikha Sharma (West Virginia University)

NETL Manager: Bruce Brown

Sandia National Laboratories is a multimission laboratory managed and operated by National Technology & Engineering Solutions of Sandia, LLC, a wholly owned subsidiary of Honeywell International Inc., for the U.S. Department of Energy's National Nuclear Security Administration under contract DE-NA0003525.

Unlock Nanopores In Shale Matrix

Nanopores accounts for > 90% of total porosity in shale. This work aims to understand fluid behaviors in shale nanopores and explore possible engineering approaches to unlocking these nanopores such that a long-term performance of a well can be improved (i.e. the slope of a decline curve can be minimized).

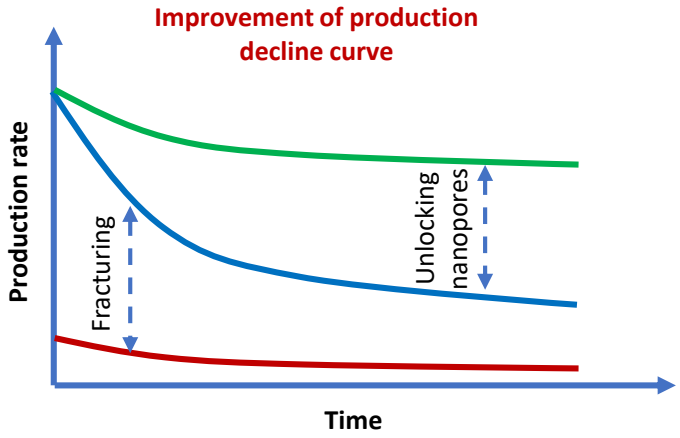

Oil/gas extraction process:

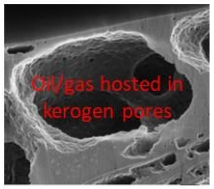

Oil/gas release from kerogen pores (Pore size: **nanometer** scale)

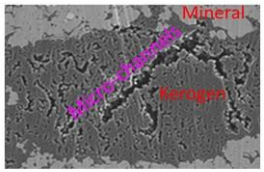

Fluid flow from kerogen via **nano- or micro**-channels (Channel size: nanometer to micrometer scale)

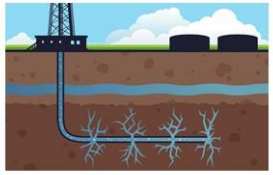

Fluid flow into hydraulic fractures and then to production well (Channel size: **millimeters** to decimeters)

Nanopores in shale matrix limit gas/oil release because fluid flux ∝ (channel size)^3.

What makes unconventional reservoirs unconventional? Fluid properties in shale nanopores are different those in conventional reservoirs (i.e. in bulk systems).

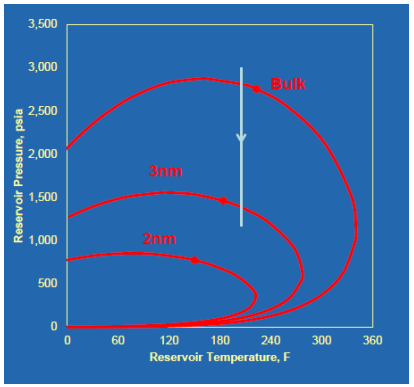

Akkutlu, 2013

Publications

- Xiong, Y., Wang, Y. & Olivas, T. (2015) Experimental Determination of P-V-T-X Properties and Sorption Kinetics in the CO_2-CH_4-H_2O System under Shale Gas Reservoir Conditions: Part One, P-V-T-X Properties, Sorption Capacities and Kinetics of Model Materials for CO_2-CH_4 Mixtures to 125°C , **High Temperature Aqueous Chemistry**, HiTAC-II Workshop, Heidelberg, April 16, 2015.
- Ho, T. A., Criscenti, L. J. & Wang, Y. (2016) Nanostructural control of methane release in kerogen and its implications to wellbore production decline. **Scientific Reports** 6, 28053; doi: 10.1038/srep28053.
- Weck, P. F., Kim, E. & Wang, Y. (2016) van der Waals forces and confinement in carbon nanopores: Interaction between CH_4, COOH, NH_3, OH, SH and single-walled carbon nanotubes. **Chem. Phys. Lett.** 62, 22-26.
- Cristancho, D., Akkutlu, I.Y., Criscenti, L.J., Wang, Y. (2016) Gas storage in model kerogen pores with surface heterogeneities, **SPE**-180142-MS, DOI: 10.2118/180142-MS.
- Wang, Y. (2017) On subsurface fracture opening and closure. **J. Petrol. Eng.** 155, 46-53.
- Weck, P. F. Kim, E., Wang, Y. et al. (2017) Model representation of kerogen structures: An insight from the density functional theory. **Scientific Reports,** 7, DOI:10.1038/s41598-017-07310-9.
- Ho, T. A., Greathouse, J. A., Wang, Y, and Criscenti, L. J. (2017) Atomistic structure of mineral nano-aggregates from simulated compaction and dewatering. **Scientific Reports**, 7, 15286.
- Ho, T. A., Wang, Y., Criscenti, L. J. & Xiong, Y. (2017) Differential retention and release of CO_2 and CH_4 in kerogen nanopores: Implications to gas extraction and carbon sequestration. **Fuel**, 220, 1-7.
- Ho, T. A. Wang, Y. and Criscenti, L. J. (2018) Chemo-mechanical coupling in kerogen gas adsorption/desorption. **Phys. Chem. Chem. Phys.**, 20, 1239.
- Ho, T. A, Wang, Y. et al. (2018) Supercritical CO2-induced atomistic lubrication for water in a rough hydrophilic nanochannel. **Nanoscale,** 10, 19957.
- Ho, T. A., Wang Y. (2019) Enhancement of oil flow in shale nanopores by manipulating friction and viscosity. **Phys. Chem. Chem. Phys.**, 21, 12777.
- Wang, Y. (2019) From nanofluidics to basin-scale flow in shale: Tracer investigations, In: **Shale Subsurface Science and Engineering,** https://doi.org/10.1002/9781119066699.ch3 (book chapter).
- Ho, T. A., Wang, Y. (2020) Pore size effect on selective gas adsorption and transport in shale nanopores, **J. Natural Gas Sci. Engineering** (available online).
- Ho, T. A., Wang, Y., Jove-Colon, C. F., Coker, E. N. (2020) Fast Advective Water Flow in Clay Interlayers, **ACS Nano** (in revision).
- Xu et al. (2020) Interaction of kerogen with brine-saturated supercritical carbon dioxide (CO2) and its implications to geologic carbon sequestration and enhanced oil/gas recovery. **Inter. J. Coal Geol.** (in revision).
- Xu, G., Wang, Y., Ho, T. A. (2020) Non-elastic behavior of kerogen upon gas adsorption/desorption, **Scientific Reports** (ready for submission)

Integrated method for construction of kerogen molecular structures

Elemental composition

NMR

FTIR

SANS

XRD

Elimination of mineral interference

MD
AIMD

Elimination of unphysical bonds

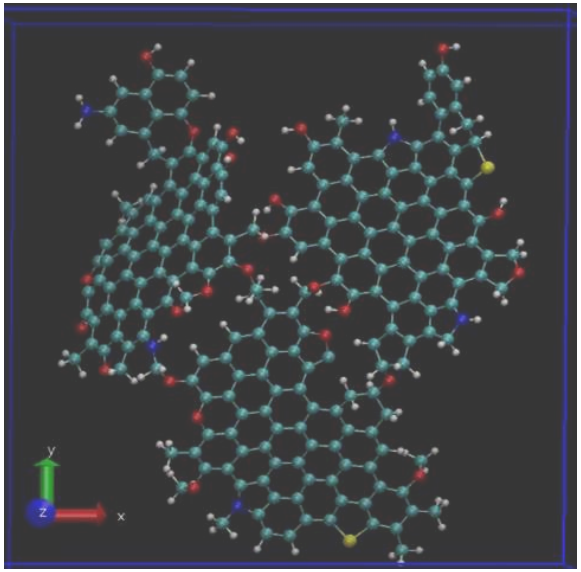

NMR Structural parameters	MarK	MIP-3H MT
Aromatic C %	90	89
Protonated C %	7	43
Bridgehead C %	60	33
Alkyl substituted aromatic C %	23	12
Aliphatic C %	5	10
Alcohol/ether C %	1	2
C (Carbons/cluster)	54	19
Cn'	0.25	0.85
FAA	0.25	0.15
Sp2/SP3 carbon	19	8.6
VRo (Vitrinite reflectance)	2.2*	2.9

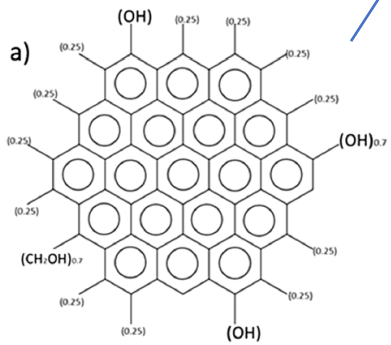

MarK

Effect of pyrite on NMR measurements

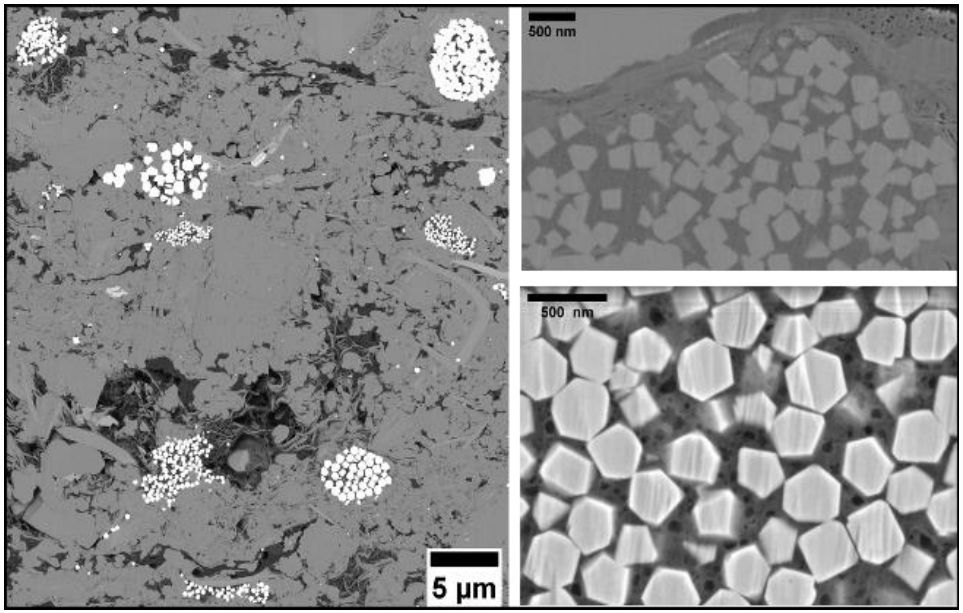

MarK sample
with 49% pyrite

Pyrite in nano-meter scale crystals are closely inter-associated with kerogen (dark color) which makes harder to remove pyrite from kerogen completely, thus the interference of pyrite cannot be ignored.

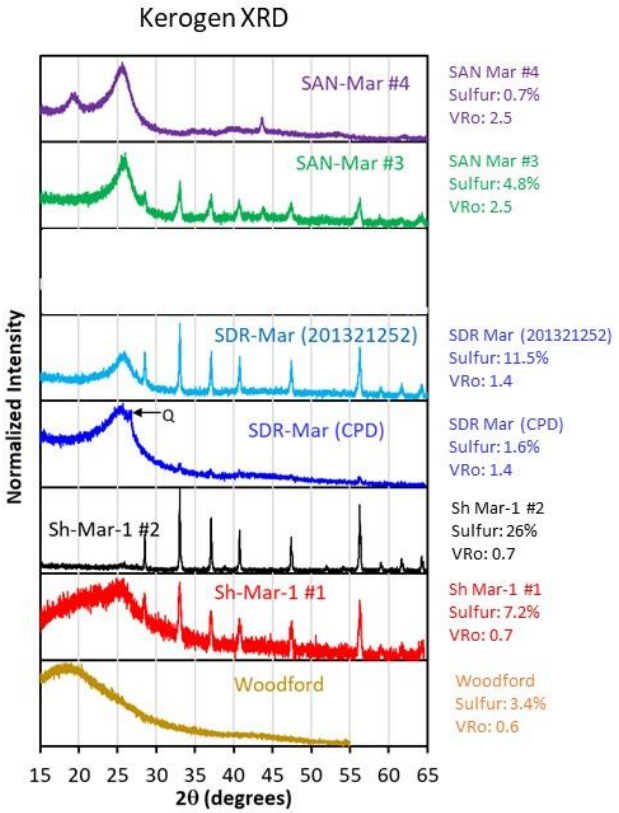

Pyrite interference causes underestimate aliphatic fraction.

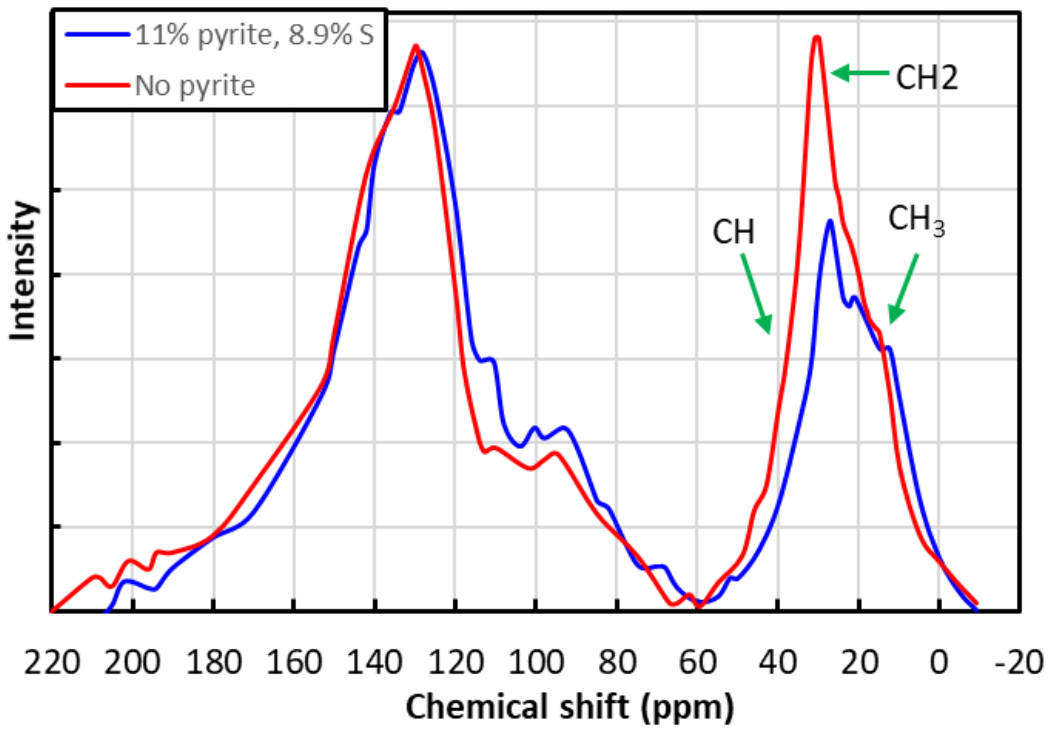

CP/MAS ^{13}C NMR spectra of the same kerogen before pyrite removal (blue) and after the removal of pyrite (red) from Bazhenov Shale. Modified from Galukhin et al. (2017)

C13 NMR data using multi-contact cross polarization (MC-CP) method

		Woodford	Sh MAR-1 #1	Sh MAR #2	SDR MAR (CPD)	SDR Mar (201321252)	San Mar #1	San MAR #2	San MAR #3	San MAR #4	Mark[b]	MIP-3H MT[d]
Vitrinite Reflectance (VR0)		0.63%	0.7%	0.7%	1.4%	1.4%	2.2%	2.2%	2.2%	2.2%	2.2%	2.9%
Sulfur by IC analysis		3.39%	7.2%	26.0%	1.6%	11.5%	1.5%		4.8%	0.7%		
Sulfur by elemental analysis		2.73%	6.8%	25.7%	3.0%	8.7%					26.3%	
Sulfur from pyrite calculated from iron		0.33%	6.1%	24.5%	0.7%	10.4%	0.27%		4.1%	0.02%		
Carbon		73.91%	76.3%	43.1%	81.7%	71.9%	85.5%	86.0%	72.1%	79.6%	36.3%	
Hydrogen		7.59%	5.9%	3.2%	3.7%	3.0%	3.0%	3.4%	2.9%	3.2%	1.4%	
Oxygen		8.40%	3.5%	3.1%	5.1%	5.2%	5.6%	5.9%	8.6%	7.7%	5.3%	
Nitrogen		2.67%	1.9%	1.2%	2.4%	2.2%	1.7%	1.6%	1.4%	1.6%	0.7%	
Iron (ICP-MS)		0.29%	5.4%	21.4%	0.62%	9.1%	0.24%		3.6%	0.02%	23%[c]	
Total[a]		95.6%	100.0%	98.0%	96.5%	100.1%	97.4%	96.8%	93.4%	92.7%	93.0%	
Pyrite		0.6%	11.5%	45.9%	1.3%	19.5%	0.5%		7.7%	0.0%	49.3%	
H/C atomic ratio		1.23	0.92	0.89	0.54	0.51	0.42	0.47	0.48	0.48	0.46	
O/C atomic ratio		0.09	0.03	0.05	0.05	0.05	0.05	0.05	0.09	0.07	0.11	
NMR structural parameters	range	Chemical shift (ppm)										
Total Aromatic carbon (%)	(90 – 165)	25.0	49.0	47.8	80.5	83.2	87.6		88.2	85.4	90	89
Total Aliphatic carbon (%)	(0 – 90)	73.7	49.0	51.9	19.2	16.8	12		10.8	14.1	5	10
Total Alkyl (%)	(0-60)	72.1	48.9	50.9	18.6	16.5	11.1		9.6	13.2		
Aldehyde and ketone (%)	(190-240)	0.2	0.1	0	0.1	0	0		0.3	0		
Carboxy and amide (%)	(165-190)	1.1	0.3	0.3	0.3	0	0.4		0.7	0.5	5	
O-substituted aromatic (%)	(150-165)	1.7	1.5	1.2	1	1.4	1		1	1.1		
Alkyl substituted aromatic (%)	(135-150)	6.1	10	9.5	11.4	13.8	10.3		8.9	10.4	23	12
Protonated aromatic (%)	(90-165)	6.1	21.8	21.6	39.7	39.7	44.4		44.4	44.7	7	43
Non-protonated aromatic (%)	(90-165)	18.9	27.2	26.2	40.8	43.5	43.2		43.8	40.7	83	45
Bridgehead aromatic carbon (%)	(90-165)	11.1	15.7	15.5	28.4	28.3	31.9		33.9	29.2	60	33
O-substituted alkyl (%)	(60-90)	1.6	0.1	1	0.6	0.3	0.9		1.2	0.9		
-CH, -CH2 (%)	(25-60)	55.4	31.8	34.5	8.9	9.2	5.3		4.2	7.2		
-CH3 (aliphatic + aromatic) (%)	(0-25)	16.7	17.1	16.4	9.7	7.3	5.8		5.4	6		
Mole fraction of bridgehead carbon		0.44	0.32	0.32	0.35	0.34	0.36		0.38	0.34	0.67	0.37
Fraction of aromatic carbons with attachments		31.2	23.5	22.4	15.4	18.3	12.9		11.2	13.5	25.6	15
Average aliphatic carbon chain length		12.1	4.9	5.5	1.7	1.2	1.2		1.21	1.36	0.22	0.85

a sulfur content using elemental measurement if available, if not using value by IC measurement; b Bousige et al. (2016); c calcuated from elemental sulfur content; d Agrawal and Sharma (2020)

Using MC-CP method eliminates the pyrite interference.

Kerogen XRD as a new structural/maturity indicator?

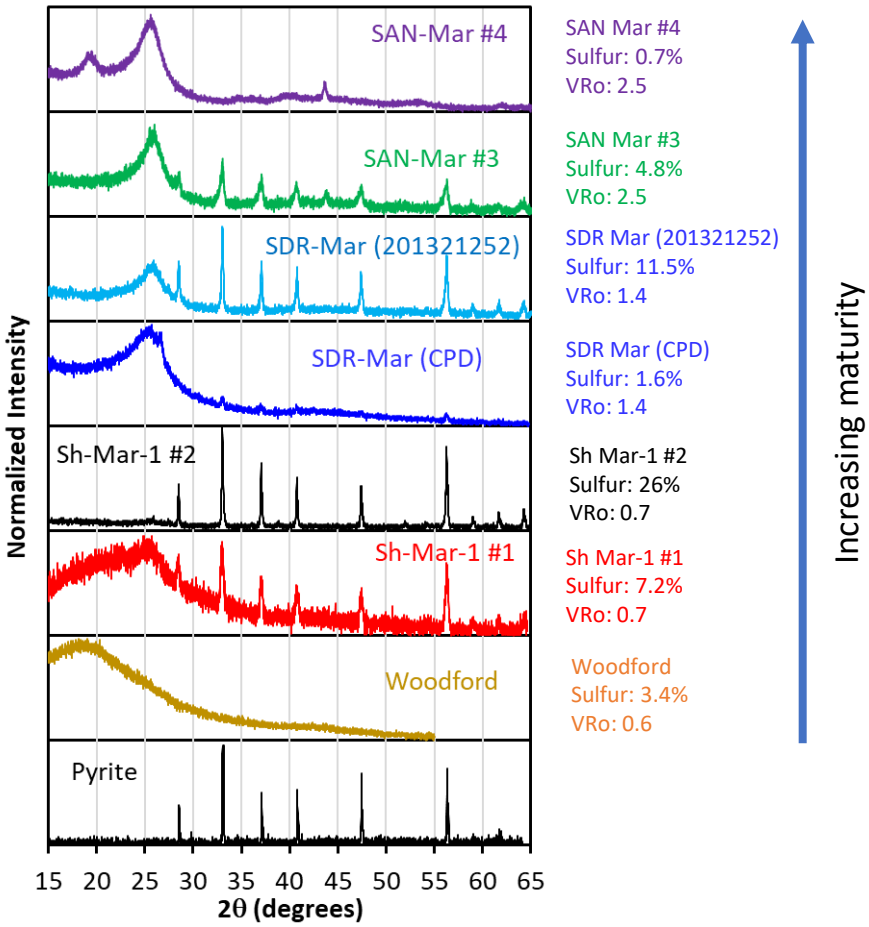

SAN Mar #4
Sulfur: 0.7%
VRo: 2.5

SAN Mar #3
Sulfur: 4.8%
VRo: 2.5

SDR Mar (201321252)
Sulfur: 11.5%
VRo: 1.4

SDR Mar (CPD)
Sulfur: 1.6%
VRo: 1.4

Sh Mar-1 #2
Sulfur: 26%
VRo: 0.7

Sh Mar-1 #1
Sulfur: 7.2%
VRo: 0.7

Woodford
Sulfur: 3.4%
VRo: 0.6

Increasing maturity

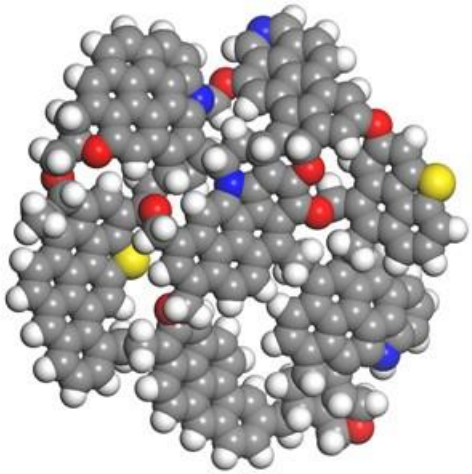

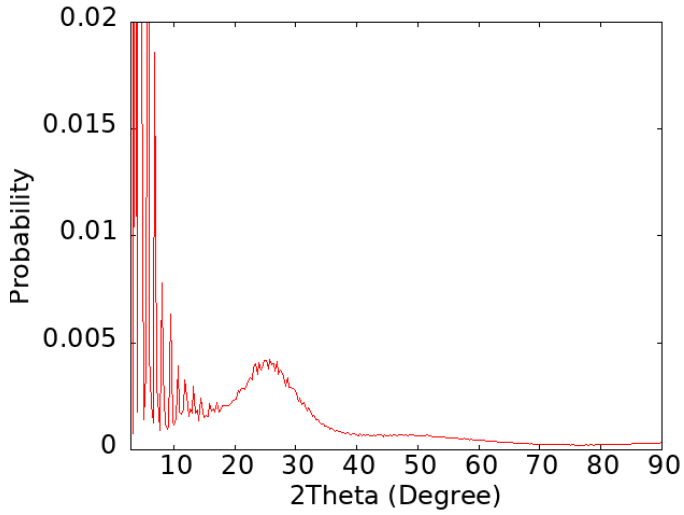

XRD curve calculated over-mature kerogen from MD simulations

Non-elastic swelling of over-mature kerogen

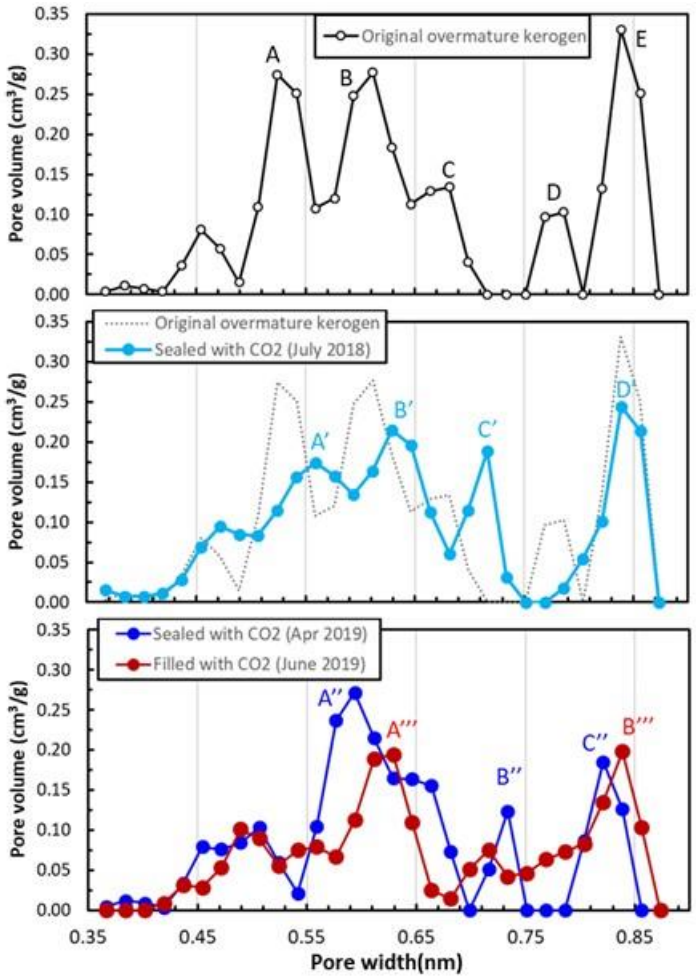

Experiments: Expose kerogen to 1 atm CO_2 and then measure pore size changes.

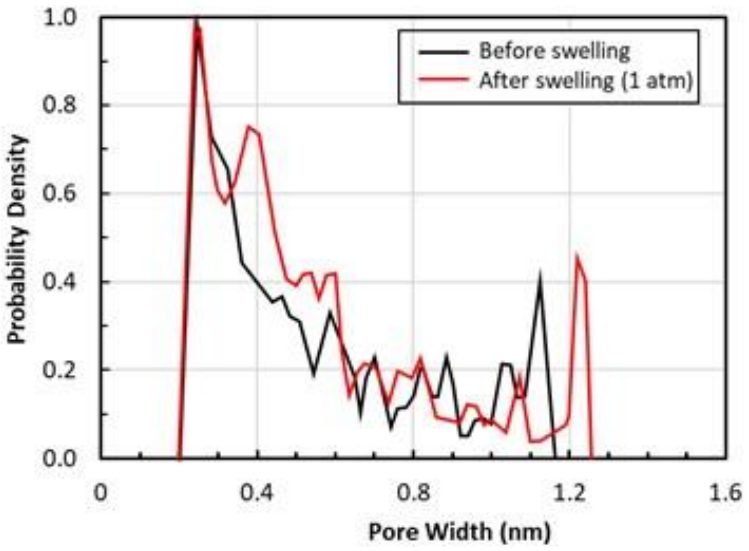

MD simulation

Peak shift:
A → A' → A'' → A''', B → B' → B'' → B''', C → C' → C'' and D → D'

- Strong mechano-chemical coupling.
- Kerogen is mechanically compliant and swelling is irreversible.
  - Mechanical properties
- Implications to reservoir engineering, especially, for organic carbon-rich ductile plays.

Multicomponent gas permeation in clay nanopores: A MD study

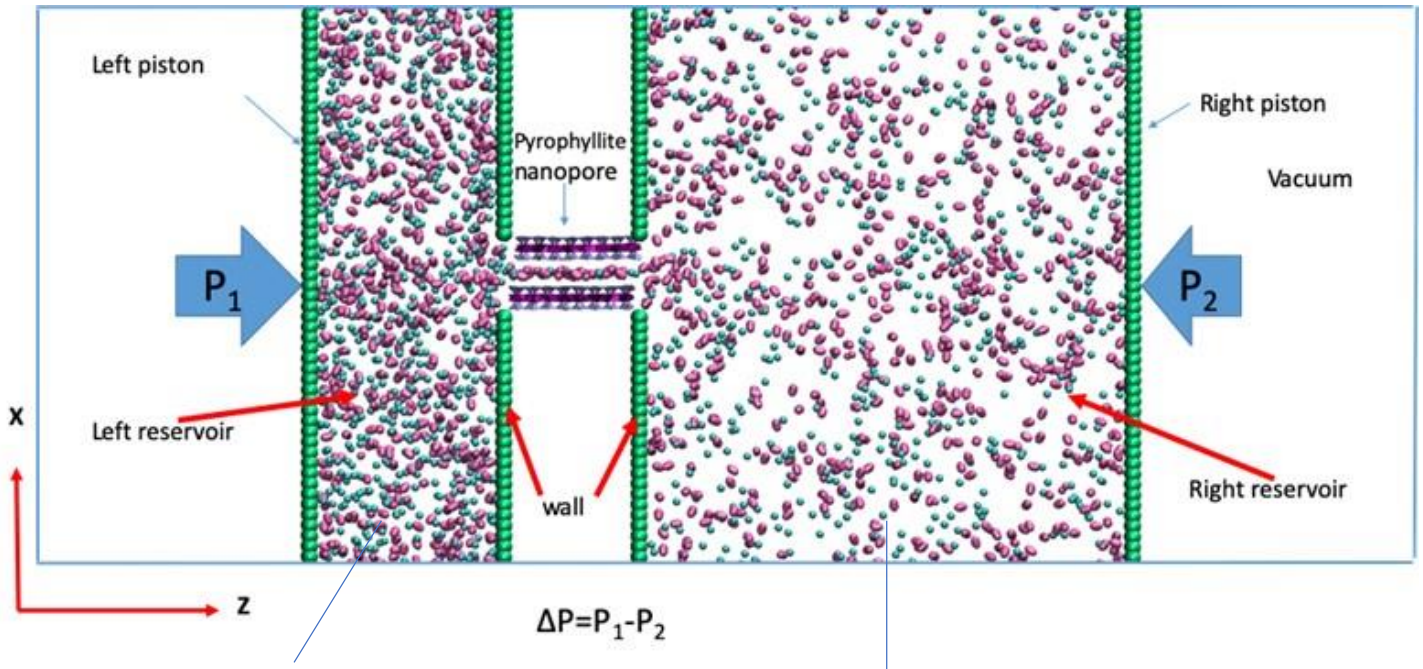

Pure gas or CH_4/C_2H_6 = 1:1

CH_4/C_2H_6 = ?

Knudsen diffusion

$$J_k = \frac{-D_k}{RT}\frac{\partial P}{\partial L} \qquad D_k = \frac{w}{3}\sqrt{\frac{8RT}{\pi M}}$$

Ho and Wang (2020)

Selective gas permeation: Pore size – 0.8 nm

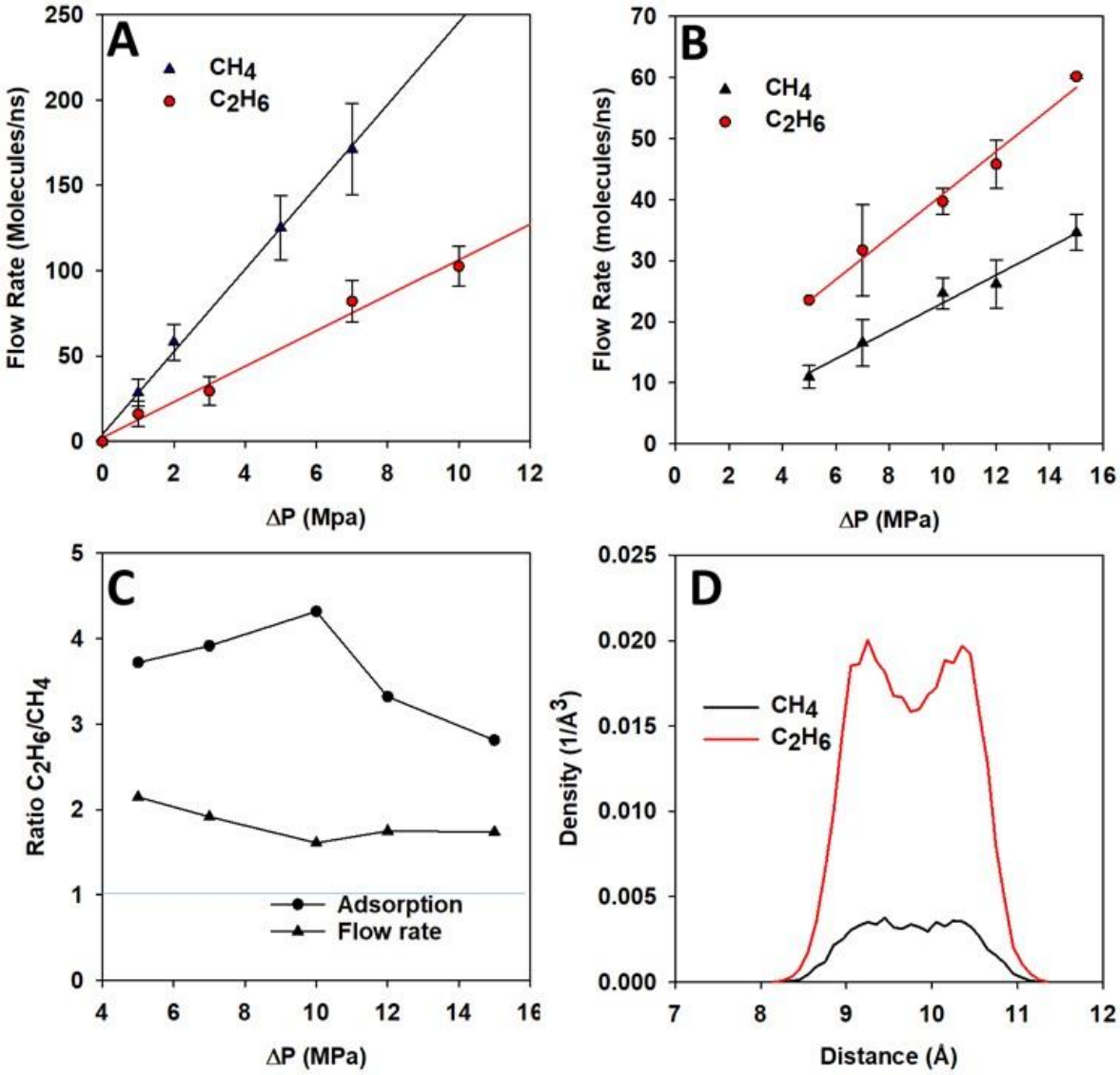

Selective gas permeation: Pore size – 1.8 nm

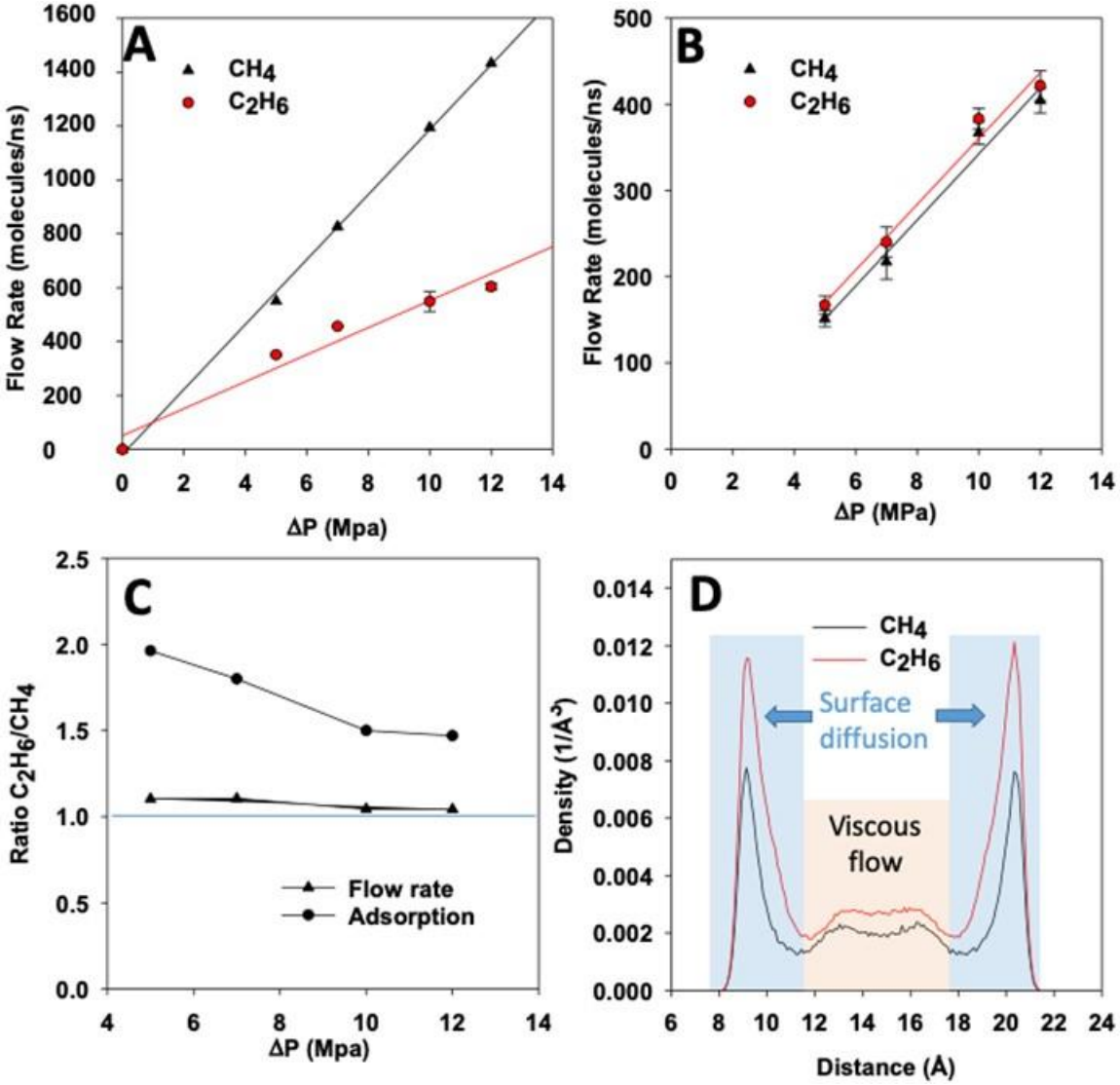

Implications

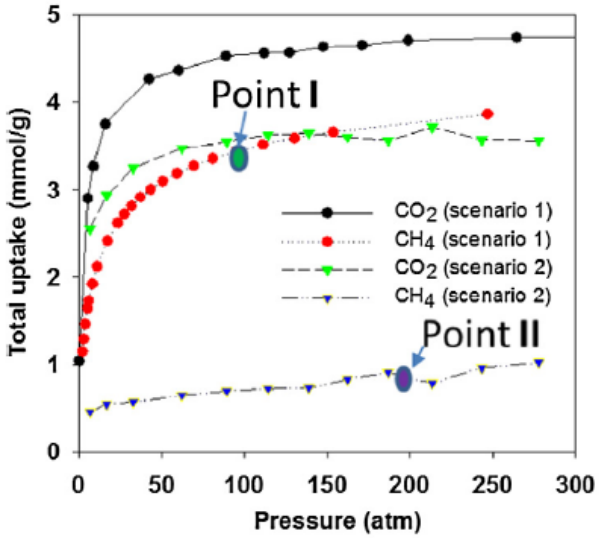

Ho et al. (2018)

- Long puzzling observation: Shale gas rich in CH_4 but depleted in CO_2.
  - Preferential CO_2 expulsion during kerogen maturation
- Continuum-scale modeling
  - Inadequacy of existing approaches: Knudsen diffusion
  - Accounting for surface sorption and surface diffusion.
- Monitoring
  - Use compositional evolution to monitor reservoir status.

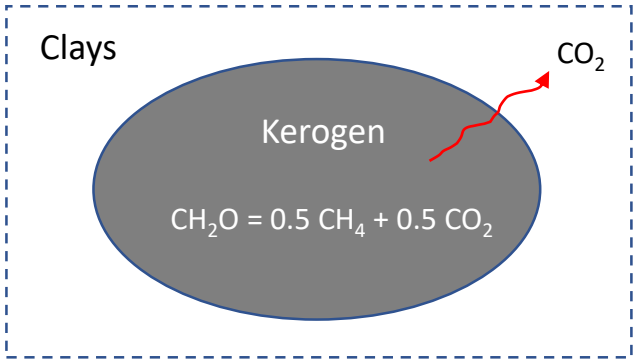

Table 1. *Apparent transport diffusion coefficients* D_i^{at} *(*m^2/s*)*

Pore size	Pure gas		Binary mixture	
	CH_4	C_2H_6	CH_4	C_2H_6
8 Å	2.149E-7	9.367E-8	2.112E-8	3.214E-8
13 Å	2.927E-7	1.108E-7	8.251E-8	9.268E-8
18 Å	4.914E-7	2.045E-7	2.153E-7	2.164E-7

Water transport in clay interlayers

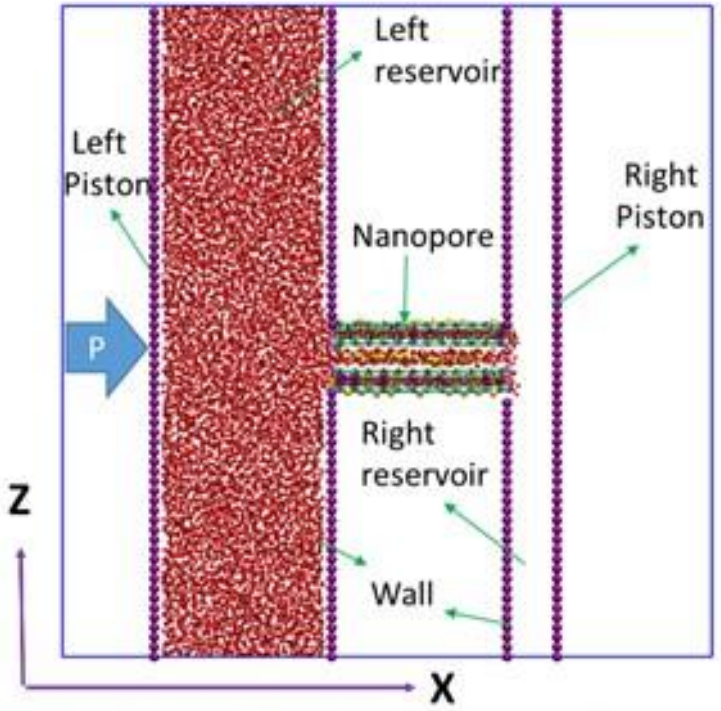

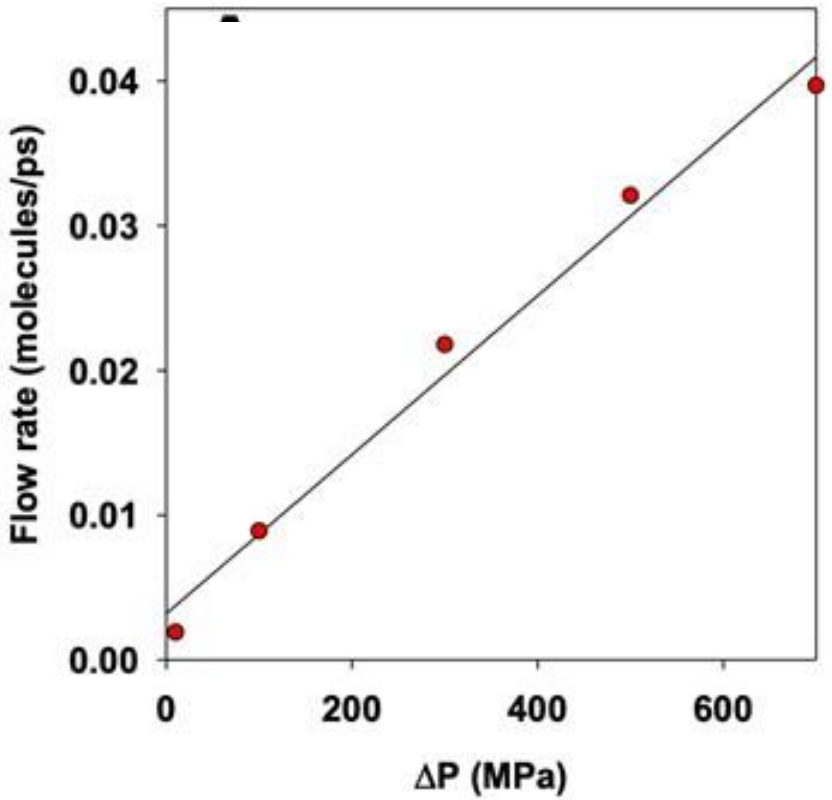

$$\Delta P\ (MPa) = -135.02 \ln(RH)$$

Relative humidity

Darcy's law still applies!

Advective water flow in clay interlayers

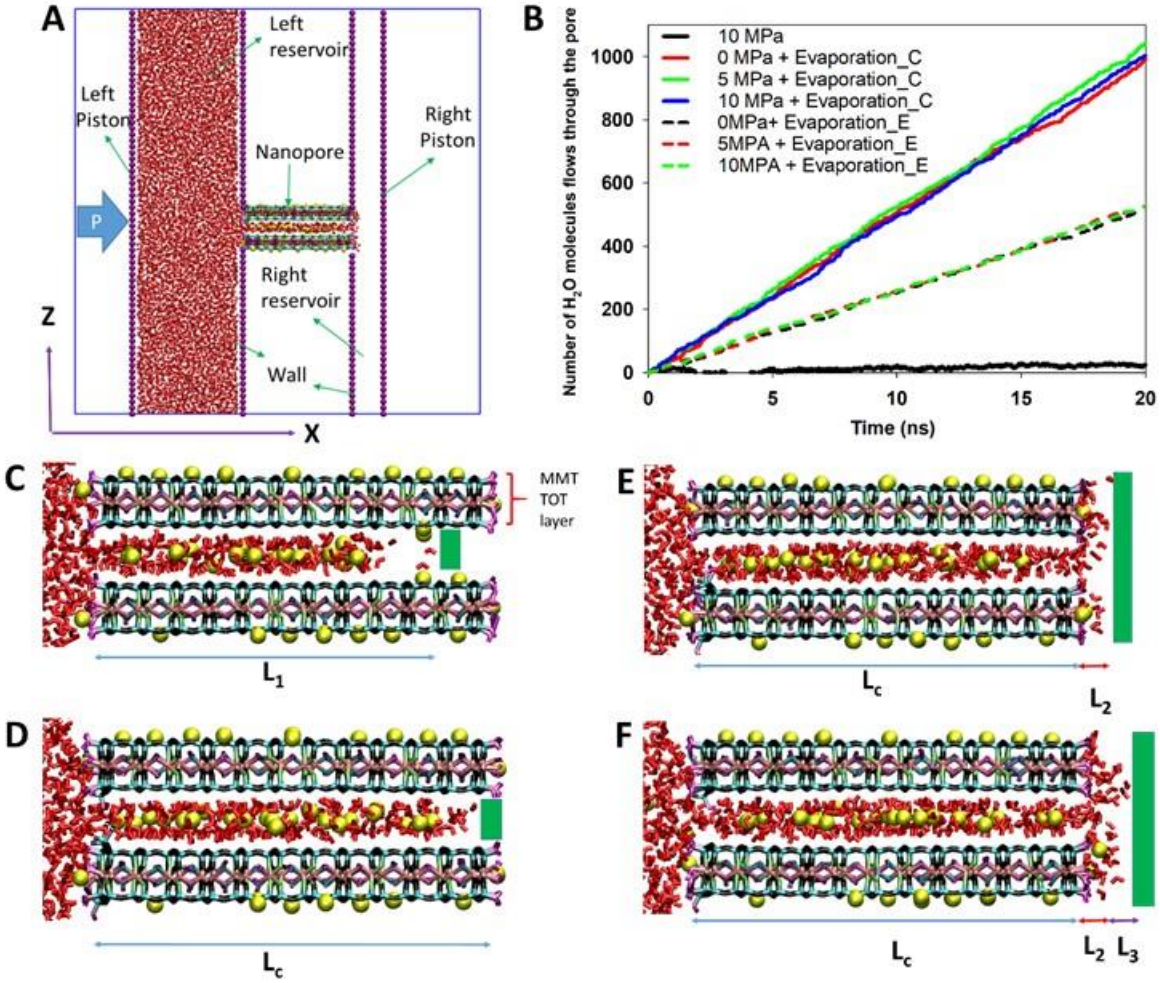

Fast advective water flow in clay interlayers

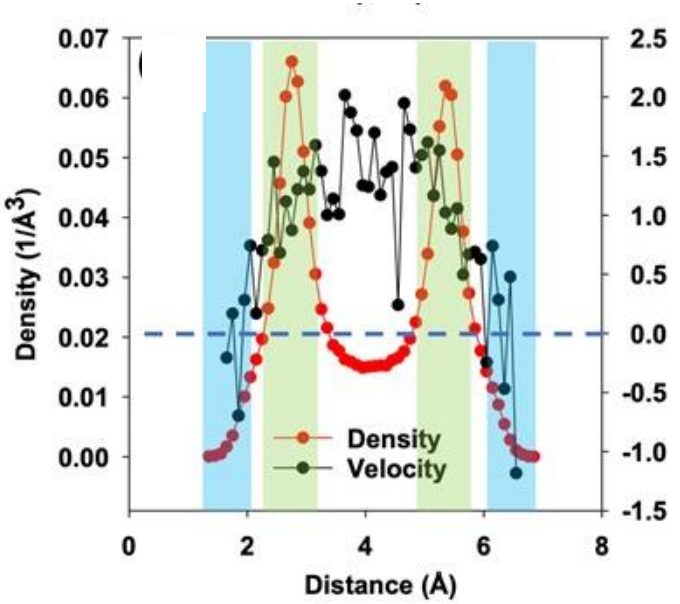

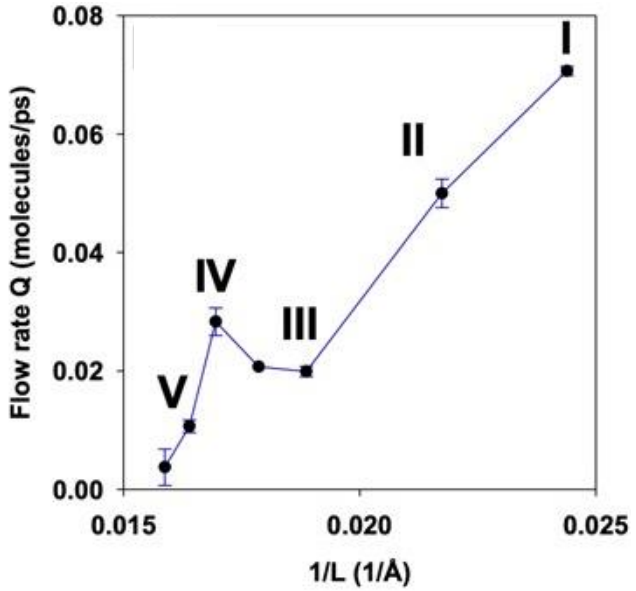

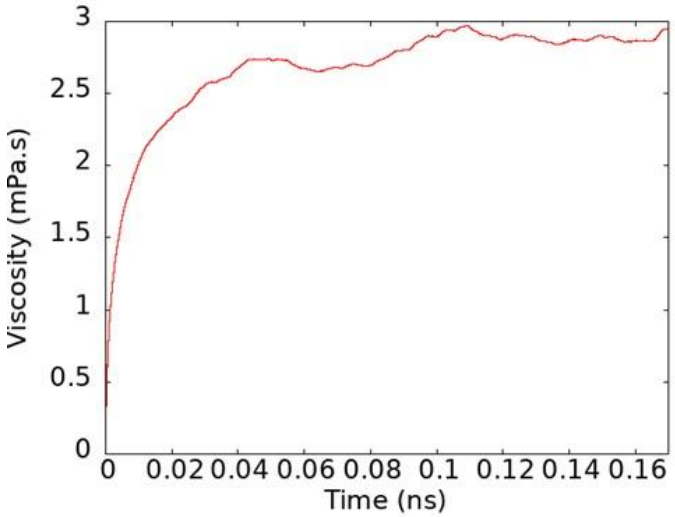

- Evaporation (~700 MPa) can drive fast advective water flow through a clay interlayer the channel.
- Flow velocity
  - ~ 0.88 m/s for a 4.6 nm long channel
  - For 2 μm particle: 95 μm/s
- Viscosity of water confined in narrow channel is ~3 times higher than bulk viscosity

Fast advective water flow in clay interlayers

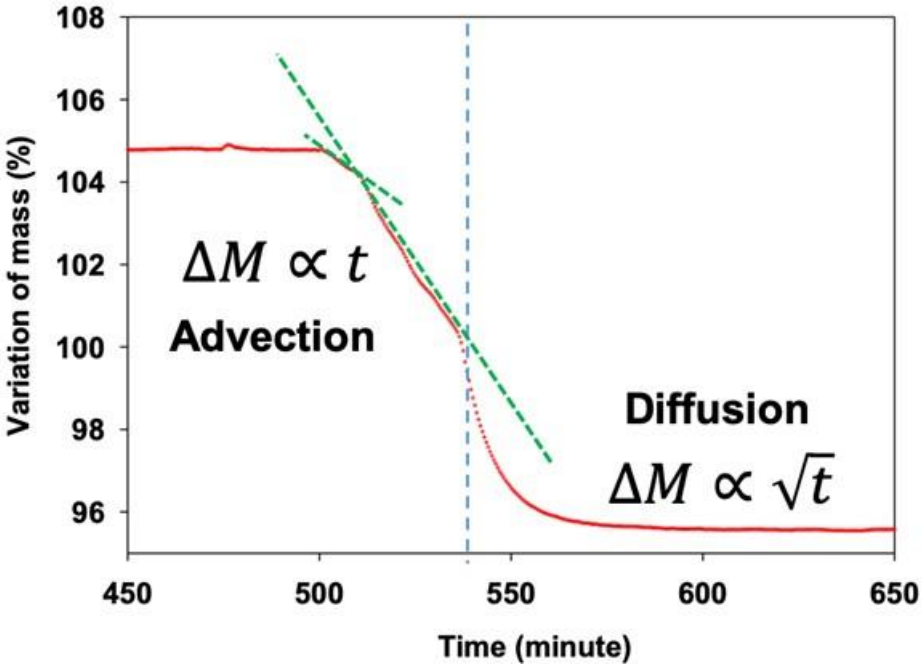

Dehydration of < 2 μm bentonite measured with thermo-gravimetric (TGA) analysis.

Implications:

- Water imbibition during hydrofracturing
- Well treatment (removal of water skin)
  - Dry supercritical CO_2?

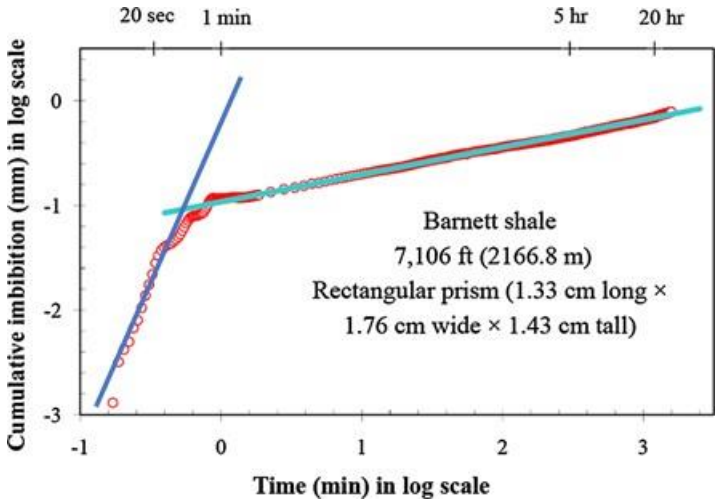

Liu et al. (2015)

Emergent transport properties in nanopores: Isotopic fractionation

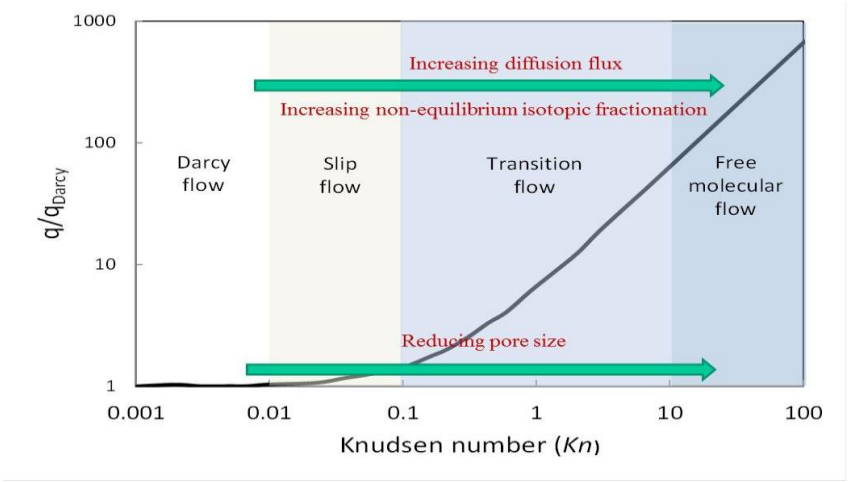

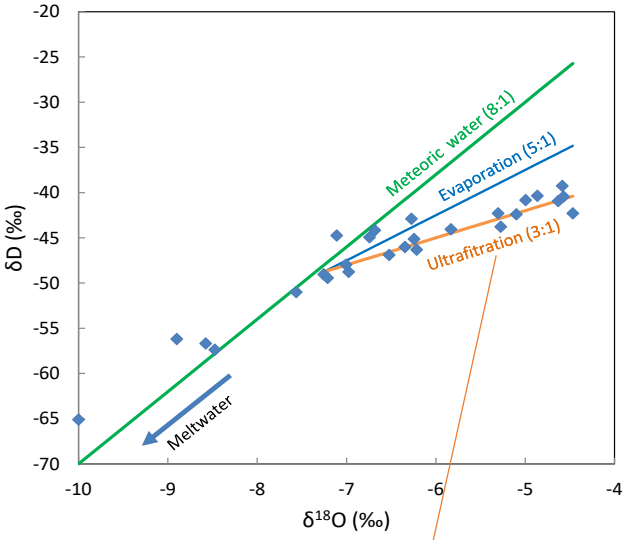

Conventional reservoir

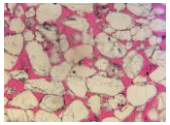

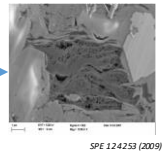

SPE 124253 (2009)

Shale formation

$$k_{app} = \frac{2r}{3RT}\left(\frac{8RT}{\pi M}\right)^{1/2} + \left[1 + \left(\frac{8\pi RT}{M}\right)^{1/2}\frac{\mu}{pr}\left(\frac{2}{\alpha} - 1\right)\right]\frac{cr^2}{8\mu}$$

M - Molecular weight

Mass dependent transport

Wang (2019)

Effect of nanoconfinement & Ultrafiltration in Shale Gas/oil Field: Isotopic Evidence

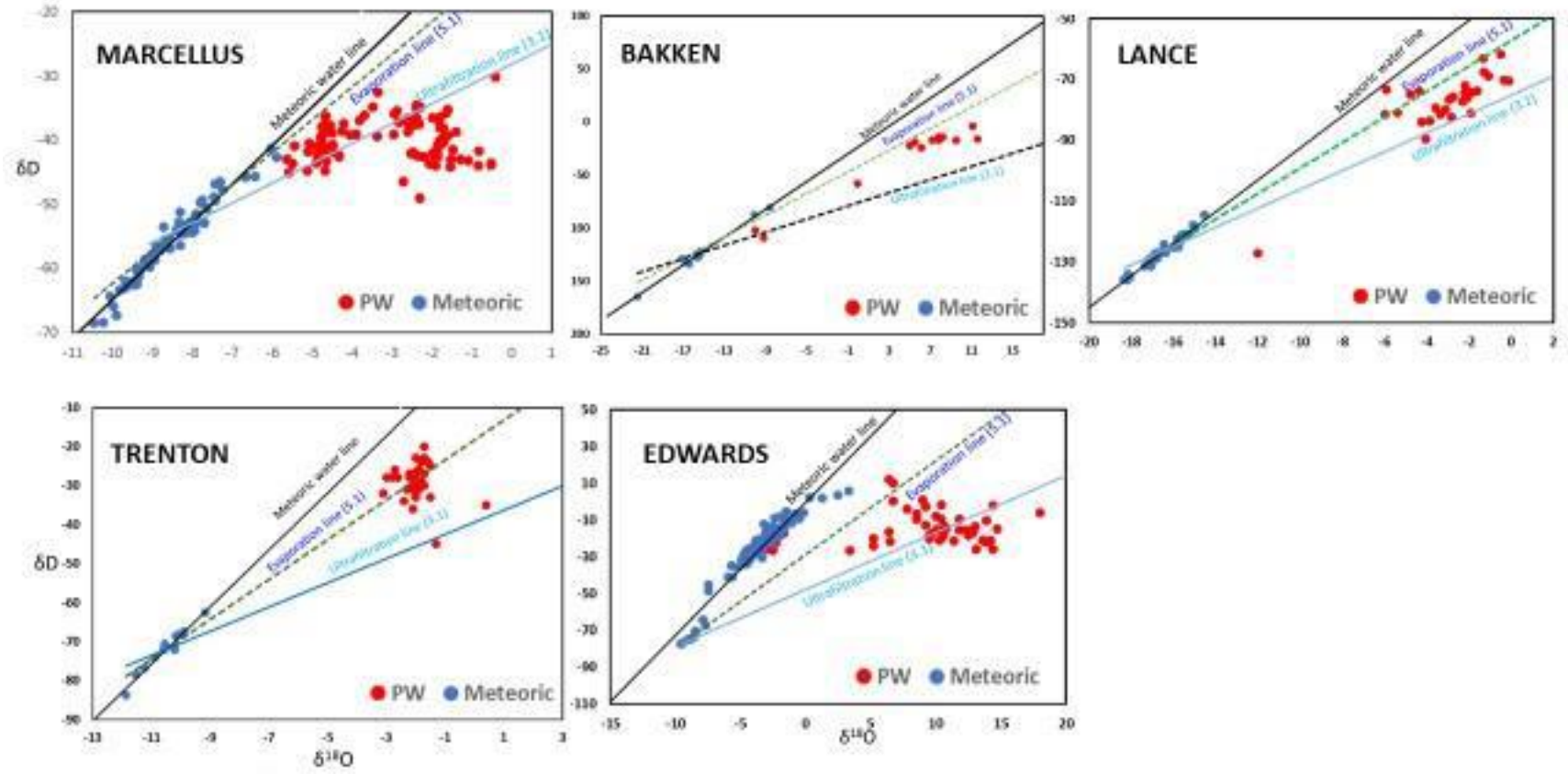

Nonlinear dynamics of fluid flow in deformable low permeability media: Porosity waves

$$\frac{\partial \phi}{\partial t} = \nabla \cdot (kf\phi^2 \nabla P)$$

Continuity for fluid

$$\frac{\partial \phi}{\partial t} = \lambda[\frac{R_d E}{2G_d^2}\tau^2 + P - I - (\phi - \phi_0)E]$$

Shear induced dilatancy

$$f = \frac{\alpha \tau^n \phi^m}{1 + \alpha \tau^n \phi^m}$$

$$\tau = \frac{G_d \sqrt{J}}{G_d - (f + \beta \nabla^2 f)(G_d - G_w)}$$

Stress partitioning/fluid-induced weakening

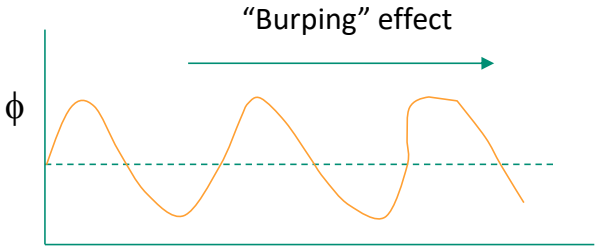

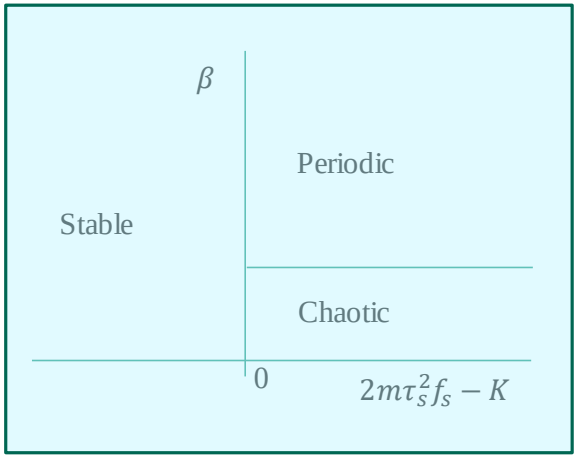

Wang et al. (2020)

New mechanism that can potentially change our general perception (and therefore manipulation) of fluid flow in unconventional reservoirs.

Results and implications

- Non-elastic swelling of kerogen upon gas adsorption/desorption.
  - Strong mechano-chemical coupling must be taken into account in a reservoir-scale simulation.
- Kerogen characterization and development of a new paradigm for structural model reconstruction
  - "Realistic" kerogen models, benchmarked and verified with experimental measurements, are critical to predict gas-in-place.
- New indicators for kerogen maturity (e.g. XRD)
  - Critical for prediction of gas-in-place and locating potential production sites.
- Selective gas permeation in clay nanochannels
  - Clays are a dominant component in shale. This result help mechanistically understand gas migration in shale matrix and provide a means for field monitoring of a production well for its recovery rate.
- Fast water advection in clay interlayers
  - Predict water imbibition during stimulation and develop a new well treatment method for removal of water skins.
- Ultrafilitration and isotopic fractionation in shale gas production
  - Develop a novel field monitoring method for shale gas production; relate field-scale observation to fluid flow processes in shale nanopores.
- Nonlinear dynamics of fluid flow in low-permeability media
  - Help develop a new stimulation strategy for shale gas production.

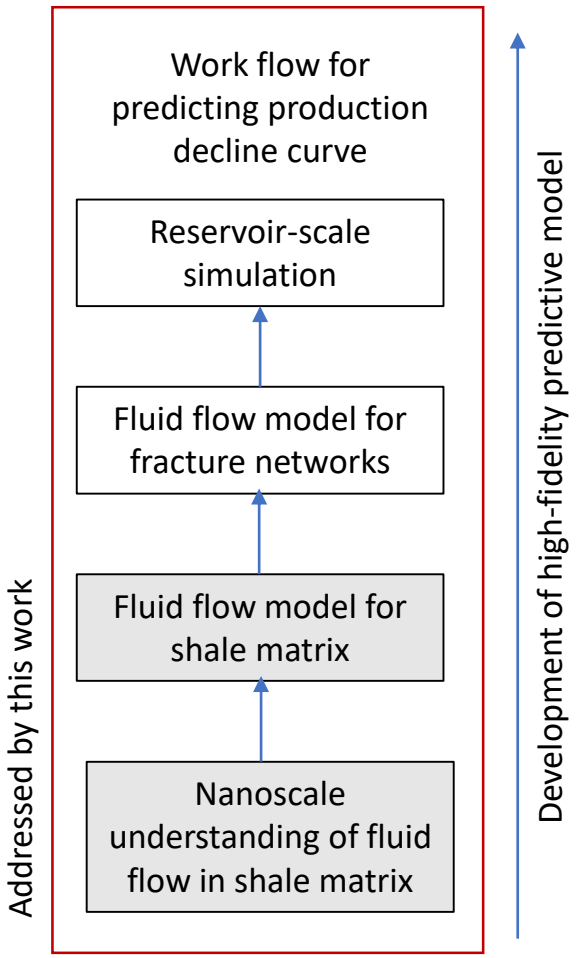

FY21 Work

Theme:
- Continue nanoscale understanding w/ focus on fluid flow;
- Extend to include other hydrocarbon components;
- Upscale fluid/material properties from nanoscale to continuum scale.

- Complete model constructions for two representative kerogens (mature and less mature).
- Update gas adsorption and release MD calculations with new kerogen structure models.
- Initiate experiments on differential gas adsorption/release from kerogen and shale samples.
- Extend MD simulations to include other chemical components (one LNG, one liquid hydrocarbon).
  - Competitive sorption
  - Fluid phase separation and transport.
- Develop EOS for one to two fluids in nanoconfinement and up-scaling the EOS.
- Understand isotope fractionation in nanoconfinement (SNL-WVU)
- Develop the nonlinear dynamic model for fluid flow in shale and related experimental capability.

Synergistics:
- SANS, fracture network modeling and reservoir scale simulations (LANL)
- Lattice Boltzmann simulations (LANL)
- Redox properties of kerogen (NETL)